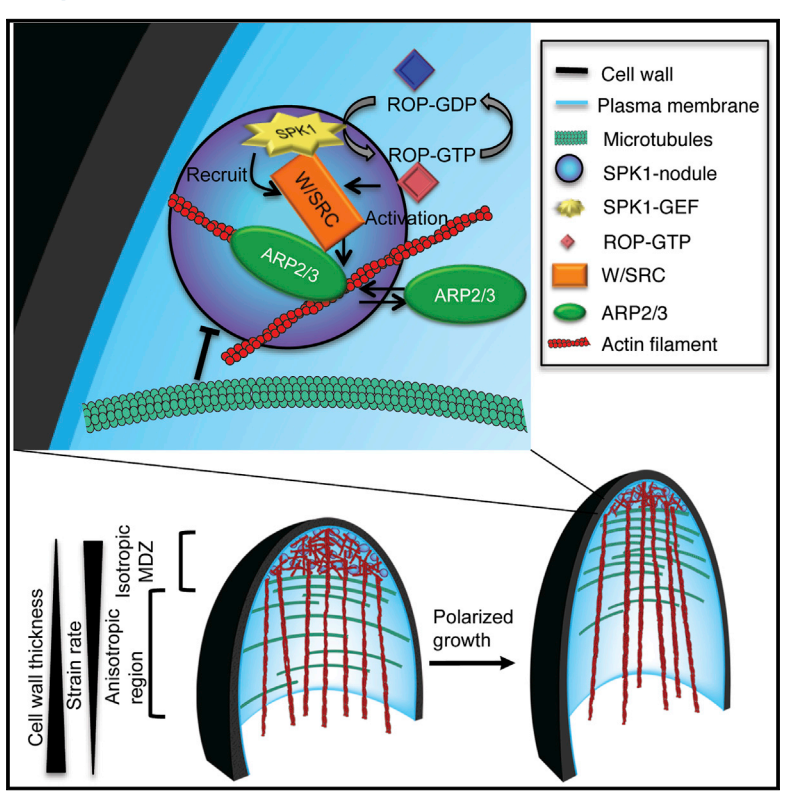
# **Current Biology**

# Microtubule-Dependent Confinement of a Cell Signaling and Actin Polymerization Control Module Regulates Polarized Cell Growth

# **Graphical Abstract**



# **Authors**

Makoto Yanagisawa, Jose M. Alonso, Daniel B. Szymanski

### Correspondence

szymandb@purdue.edu

#### In Brief

Yanagisawa et al. discover that the DOCK family GEF SPIKE1 recruits and activates actin filament nucleation machineries to generate an apical patch of cortical actin that organizes cytoplasmic transport. Microtubules confine SPIKE1 to the cell apex to generate non-overlapping cytoskeletal arrays that both pattern and respond to the cell wall.

## **Highlights**

- The ROP/Rac GEF SPIKE1 emits signals from plasma membrane-associated nodules
- SPIKE1 patterns the actin cytoskeleton by clustering and activating the WAVE complex
- Microtubules confine SPIKE1 signaling nodules within an apical microtubule-free zone
- Feedback control from the cell wall modulates cytoskeletal organization







# Microtubule-Dependent Confinement of a Cell Signaling and Actin Polymerization **Control Module Regulates Polarized Cell Growth**

Makoto Yanagisawa,<sup>1,4</sup> Jose M. Alonso,<sup>3</sup> and Daniel B. Szymanski<sup>1,2,5,\*</sup>

- <sup>1</sup>Department of Botany and Plant Pathology, Purdue University, West Lafayette, IN 47907, USA
- <sup>2</sup>Department of Biological Sciences, Purdue University, West Lafayette, IN 47907, USA
- <sup>3</sup>Department of Plant & Microbial Biology, North Carolina State University, Raleigh, NC 27695, USA
- <sup>4</sup>Present address: Department of Botany and Laboratory of Cell & Molecular Biology, University of Wisconsin-Madison, Madison, WI 53706, USA
- <sup>5</sup>Lead Contact
- \*Correspondence: szymandb@purdue.edu https://doi.org/10.1016/j.cub.2018.05.076

#### **SUMMARY**

Cell types with wildly varying shapes use many of the same signaling and cytoskeletal proteins to dynamically pattern their geometry [1-3]. Plant cells are encased in a tough outer cell wall, and growth patterns are indirectly controlled by the cytoskeleton and its ability to locally specify the material properties of the wall [4, 5]. Broad and non-overlapping domains of actin and microtubules are predicted to create sharp cell-wall boundaries with distinct mechanical properties [6] that are often proposed to direct growth patterns and cell shape [1, 6, 7]. However, mechanisms by which the cytoskeleton is patterned at the spatial and temporal scales that dictate cell morphology are not known. Here, we used combinations of live-cell imaging probes and unique morphology mutants in Arabidopsis to discover how the microtubule and actin systems are spatially coordinated to pattern polarized growth in leaf epidermal cells. The DOCK family guanine nucleotide exchange factor (GEF) SPIKE1 [8, 9] clusters and activates conserved heteromeric WAVE/SCAR and ARP2/3 complexes at the cell apex to generate organized actin networks that define general cytoplasmic flow patterns. Cortical microtubules corral punctate SPIKE1 signaling nodules and restrict actin polymerization within a broad microtubule-depletion zone at the cell apex. Our data provide a useful model for cell-shape control, in which a GEF, actin filament nucleation complexes, microtubules, and the cell wall function as interacting systems that dynamically pattern polarized growth.

#### **RESULTS AND DISCUSSION**

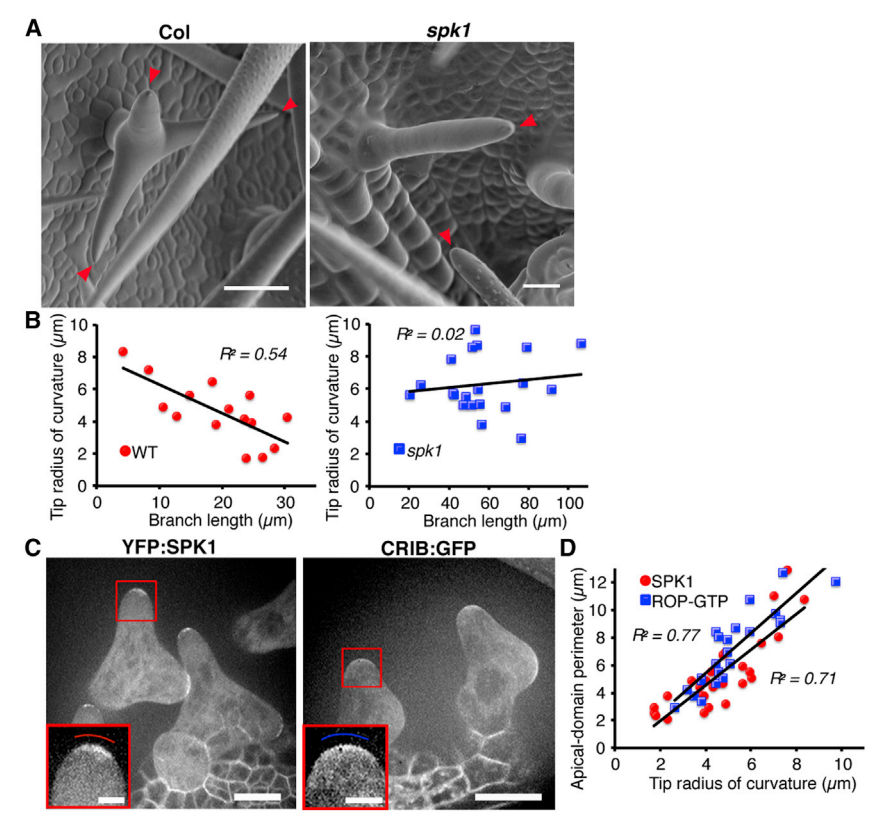
#### **SPK1 GEF Activity Is Required at the Apex to Pattern Branch Tapering**

In general, the cellular control of ARP2/3 is poorly understood; most genomes contain gene families that encode many types of ARP2/3 activators and in nearly all cases the specific guanine nucleotide exchange factors (GEFs) that transmit small GTPase signals to ARP2/3 are unknown [10]. However, in plants the situation is simplified, because ARP2/3 appears to be activated solely by the evolutionarily conserved WAVE/SCAR regulatory complex (W/SRC) [11, 12], and there is biochemical and genetic evidence that the ROP/Rac GEF SPIKE1 may transmit activating signals to W/SRC [8, 13]. SPK1 was also involved in ARP2/ 3-dependent cell tapering [6] because, like w/src and arp2/3 trichomes [11], those of spk1 had blunt branch tips that failed to taper normally during elongation (Figures 1A and 1B).

To analyze the function and dynamics of SPK1 in vivo, we generated stable yellow fluorescent protein (3X-YFP):SPK1 lines in the context of a 64 kb genomic fragment using recombineering (Figure S1A) [14]. The YFP:SPK1 fusion protein was functional because in four of four independent transformed lines with a complete T-DNA, it dominantly rescued all null spk1 mutant phenotypes (Figures S1B-S1E), and the fusion protein was intact (Figure S1F). SPK1 localized at the apex of all young trichome branches, and the geometry of the SPK1 domain scaled closely with the changing tip morphology (Figures 1C and 1D). In rare instances ( $\sim$ 5%), a relatively broad domain of SPK1 signal was observed closer to the branch base. The branch tip localization pattern resembles that of the W/SRC and ARP2/3 complexes, which reside in an apical microtubule-depletion zone (MDZ) [6].

SPK1 has GEF activity in vitro [8, 9]. To test for SPK1 GEF activity in trichome apices, we created a biosensor for active ROP by fusing the Cdc42/Rac-interactive binding domain of RIC1 with green fluorescent protein (CRIB:GFP). 45% of the branch apices (n = 56) had elevated levels of active ROP (Figure 1C; Table S1), and no such localized accumulation was observed with GFP alone (Figure S1G). These data suggest that SPK1 GEF activity at the cell apex is latent or variable, because SPK1 is a permanent resident at the apex whereas active ROP was present in only a fraction of the branches. SPK1 contributed to the apical pool of active ROP because both molecules localized to the tapering tip (Figure 1D), and the percentage of branches showing tip-concentrated CRIB:GFP signal was reduced to 24% in spk1 (Table S1). This result also indicates that other GEFs, probably plant-specific PRONE domain-containing family members [15], are active in the trichome branch tip.





#### **SPK1** Recruits and Activates W/SRC at the Branch Apex

The localization of SPK1 to the branch apex is consistent with the GEF having a role in the recruitment and/or activation of the W/SRC and ARP2/3 complexes. The localization of SPK1 was compared with those of BRK1/HSPC300:YFP and ARPC5:GFP, which are validated live-cell probes for the functional W/SRC and ARP2/3 complexes, respectively [6, 16-18]. Like SPK1, the W/SRC and ARP2/3 complexes were clearly tip localized (Figure 2A). A previous analysis reported BRK1 and the ARP2/3 complex at the apex in 66% and 28% of the trichome branches, respectively [6] (Table S1). A punctate distribution of SPK1 was more apparent in face-on views of the branch apex (Figure 2B), and the W/SRC and ARP2/3 complexes also had punctate distributions that were indistinguishable from SPK1 in terms of both their size and density (Figures 2C and 2D). Unfortunately, we could not conduct two-color live-cell imaging of SPK1 and BRK1 or ARP2/3, because mCherry-fusion proteins of BRK1 and ARPC5 were too dim to resolve at the trichome apex. Given the localization data above, and that SPK1 genetically and physically interacts with W/SRC [8, 13], it is very likely, but not proven directly, that all of these proteins are functioning at the same subcellular location.

Nonetheless, it was clear that SPK1 was required to cluster W/SRC normally, because in the spk1 background only 17% of the branches had a normal distribution of BRK1 at the apex (Figure 2E; Table S2). The majority of spk1 branches had no cortical BRK1 signal, and in the remaining ~30% of spk1 branches BRK1 signal was clearly off the center axis of the cell or mislocalized to the flanking region of the apex. Therefore, Arabidopsis W/SRC has some ability to cluster near the cell

Figure 1. SPK1 Activates ROPs to Modulate Cell Shape at the Branch Apex

(A) SEM micrographs of young trichomes on wildtype and spk1 leaves. Trichome tips are marked with red arrowheads and become progressively narrow as wild-type branches elongate. Scale bars

(B) Branch tip radius of curvature plotted as a function of branch length (left, wild-type, n = 15; right, spk1, n = 20). The mutant and wild-type cells are at similar developmental stages. However, the branch length values reported for spk1 are greater because the cells are unbranched and, unlike the wild-type, the elongating cell is not divided into stalk and branch segments.

(C) YFP:SPK1 and active ROP are concentrated at the branch apex. CRIB:GFP is a biosensor that selectively binds to GTP:ROP. Areas contained within the red boxes are magnified in the insets. Scale bars represent 20 µm (5 µm in insets).

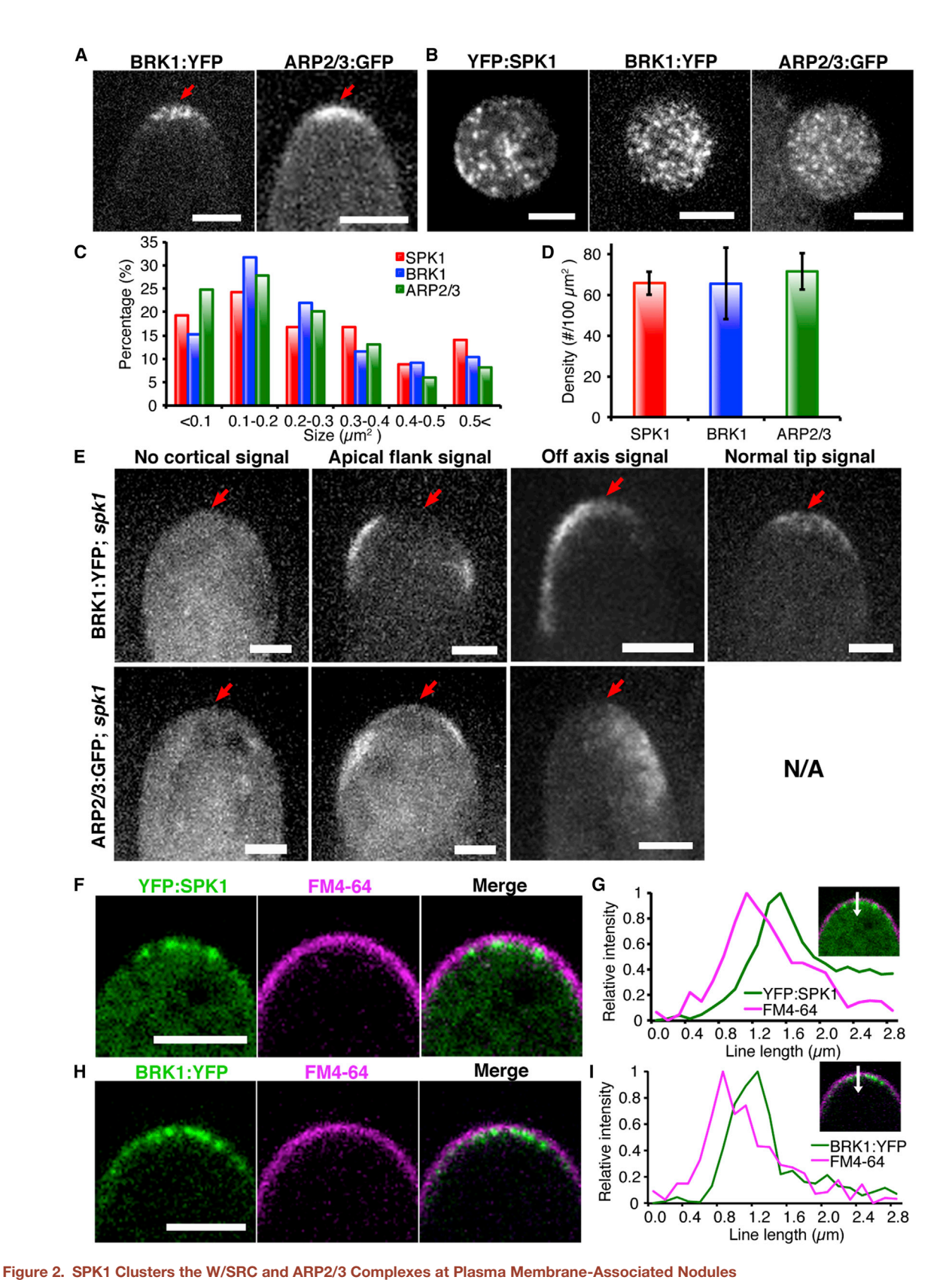
(D) The geometry of the SPK1 (red) and active ROP (blue) domains is linked to the branch tip radius of

See also Figure S1 and Table S1.

apex independent of SPK1. However, in spk1 cells, W/SRC was not effective in terms of ARP2/3 complex clustering and activation. None of the branches analyzed had a normal distribution of apical ARP2/3

complex, and among the  $\sim$ 15% that had any tip-localized ARP2/3 complex the pattern was altered in a way that mirrored the defective distribution of BRK1 (Figure 2E; Table S2). In tip-growing moss cells [19] and in the trichome apex [6], the polarized localization of the ARP2/3 complex depends on a functional W/SRC. In the spk1 background W/SRC is assembled [8] but apparently inefficient in terms of recruiting the ARP2/3 complex, because the localization defects of the ARP2/3 complex are more severe compared to BRK1 and the W/SRC (Table S2). It has previously been shown that arp2/3 mutants completely lack an apical cortical actin meshwork [6], and that null mutants for arp2/3, w/src, and spk1 all have very similar actin phenotypes in early-stage trichomes [8, 11]. Therefore, our data indicate that SPK1 recruits and channels activating signals to W/SRC to promote localized actin polymerization at the apex as the cell tapers.

We found no evidence for direct feedback control of the W/SRC or ARP2/3 complexes on the ability of SPK1 to be clustered in the cell apex, because it was tip localized in nearly every early-stage branch when either of the above complexes was mutated (Figure S2A; Table S1). However, the size of the SPK1 domain became more random in the w/src and arp2/3 mutants (Figure S2B) compared to the wild-type (Figure 1D) when graphed as a function of the changing tip radius of curvature. This is consistent with the previously reported randomized size of the MDZ in arp2/3 mutants [6], and suggests some form of feedback control between cell-wall geometry and the size and location of the MDZ. The geometries of the MDZ and ARP2/3 complex activation domains are tightly regulated during branch elongation to enable normal cell tapering. The ARP2/3-generated apical patch of



(A) Localization of BRK1:YFP and ARP2/3:GFP in wild-type trichomes. (B–D) Face-on projected views of tip-localized SPK1, BRK1, and ARP2/3 in developing trichomes (B). Size distribution (C) and density (D) of punctae. Mean ± SD (n > 160).



cortical actin orients cytoplasmic actin bundle networks to enable highly organized long-distance transport and the maintenance of cell-wall thickness gradients that enable polarized expansion [6]. As the branch elongates the apical MDZ becomes progressively constricted, and this is predicted to generate a specialized patch of cell wall at the apex with randomized cellulose fibers and isotropic mechanical properties that can mediate cell tapering [6]. Our data suggest that actin-based outputs of the W/SRC-ARP2/3 complex pathway are required to properly couple the geometries of the cell wall to the size of the SPK1-positive domain and the MDZ.

# SPK1 Punctae Are Transient Nodules that Are Associated with the Plasma Membrane

The SPK1 live-cell probe allowed us to analyze the spatial and temporal dynamics of the GEF as a function of a changing cell morphology. Knowledge on the precise origin of DOCK GEF signals is limited. They may function at the plasma membrane [18, 20] or at sub-domains of the endoplasmic reticulum [21, 22]. The SPK1 and BRK1 punctae were not obviously localized to sub-domains of the plasma membrane, because the peak signal intensities of YFP:SPK1 and BRK1:YFP were not in the plane of the plasma membrane but almost always were in contact with the plasma membrane (Figures 2F-2I, S2C, and S2D). These nodule-like structures could be a localized invagination of the plasma membrane; however, such structures are not common in electron microscopy analyses of the plant cortex. Our leading hypothesis is that nodules correspond to a distinct endomembrane compartment that is associated with the plasma membrane. An ultrastructural analysis using electron microscopy is needed to better define the membrane topology of these striking SPK1-positive structures.

The SPK1 punctae appeared to be anchored stably to a particular domain of the plasma membrane, because time-lapsed analyses showed that SPK1 punctae were relatively immobile, with most having very slow average speeds of 228 ± 156 nm/min (Figure S2E). There were maturation and destabilization phases to SPK1 punctae formation, because they often became progressively bright prior to their disappearance, and punctae size was correlated with mean particle brightness (Figures S2F–S2H). On rare occasions, punctae would detach and stream in the subcortical cytoplasm (Figures S2G and S2I; Video S1). The image data indicate that SPK1 signals originate primarily from a distributed network of nodules that are clustered within the specialized apical domain of the cell.

We were not able to precisely identify the organelles that form SPK1 nodules. In epidermal pavement cells, SPK1 is a peripheral endoplasmic reticulum (ER)-associated protein, and a sub-pool colocalizes with ER-exit site markers [21]. Using the general ER marker GFP:HDEL and a validated ER-exit site marker (YFP:SEC24A), it was clear that the ER was widely distributed in young trichomes (Figure S3A). The ER tended to occupy the

extreme branch apex, compared to an array of other organelle markers, which were excluded from the apex (Figures S3B and S3C). We tested for tip gradients of the known ER-PM (plasma membrane) contact site markers SYT1 and VAP27 (Figure S3D). Both had a broader subcellular distribution compared to SPK1. However, sub-pools of these proteins were present in the cortex at the branch apex. It remains possible that sub-pools of SYT1 and VAP27, perhaps in combination with additional proteins and lipid modifications, have specialized functions that enable SPK1 to be efficiently clustered at specific organelle domains.

For a better understanding of how individual SPK1 punctae and the apical SPK1 signaling domain as a whole are reshaped as a function of morphogenesis, the dynamics of SPK1 nodules were analyzed across wide temporal and spatial scales. In emerging branch buds, SPK1 nodules were enriched at the apex compared to the cell flank (Figure 3A). As the branch elongated, the tip radius of curvature and the cortical domain-containing SPK1 nodules were constricted at similar rates (Figure 3B; Video S2). Particle tracking analyses indicated that the total number of trackable punctae in the branch decreased in both apex and flanking regions of the cell; however, because the area of the SPK1 signaling domain was decreasing, the average density of SPK1 nodules was maintained at the apex, but not in the flank (Figures 3C and S3E-S3H). The cortex of the branch apex was specialized in terms of forming SPK1 punctae, as they formed 3.5 times more frequently in the apex compared to the flank (Figure S3I). This result suggests that a specialized endomembrane organization that efficiently promotes SPK1 clustering is present at the branch apex.

Although SPK1 was always present in the apex of developing branches (Table S1), time-lapsed analyses consistently revealed unstable SPK1 punctae appearing and disappearing at variable rates (Video S2). The lifetimes of SPK1 nodules were compared between the extreme apical region and the region labeled "interface" that was adjacent to the cell flank (Figures 3A and 3D). At both locales, the punctae varied greatly in their persistence; most appeared and disappeared within  $\sim$ 2 min, but others were trackable for over 30 min. However, at the interface region, punctae lifetimes were significantly shorter, suggesting that SPK1 nodules are destabilized near the proximal boundary of the signaling domain. The directionality of SPK1 nodule movement also differed as a function of their location: those within the apical domain tended to move slowly toward the cell tip, but the particle trajectories along the cell flank were more random (Figures 3E and S3D). This important result suggested a potential control mechanism for SPK1 nodule localization based on the known localization of cortical microtubules in this cell type.

### Microtubules Corral SPK1 Punctae within the Cell Apex

Cortical microtubules are tightly associated with the PM [23] and have the potential to act as a barrier to lateral diffusion

<sup>(</sup>E) Defined altered localization patterns of BRK1:YFP and ARP2/3:GFP in *spk1* trichomes. Apical flank signal is close to but outside of the cell apex. Off axis signal is partially at the branch apex but off center. N/A, not applicable.

<sup>(</sup>F–I) SPK1 or BRK1 punctae are resolved from the plasma membrane at the branch apex. Trichome branches expressing YFP:SPK1 (F) or BRK1:YFP (H) were stained with FM4-64 to label the plasma membrane. Intensity profiles of FM4-64 and YFP:SPK1 (G) and BRK1:YFP (I). All of the trichomes analyzed for tip localization were stage 4 cells with blunt branches with a length of less than 50 μm.

The arrows in (A), (E), (G), and (I) mark the location of the branch apex. Scale bars represent 5 µm. See also Figures S2 and S3 and Tables S1 and S2.

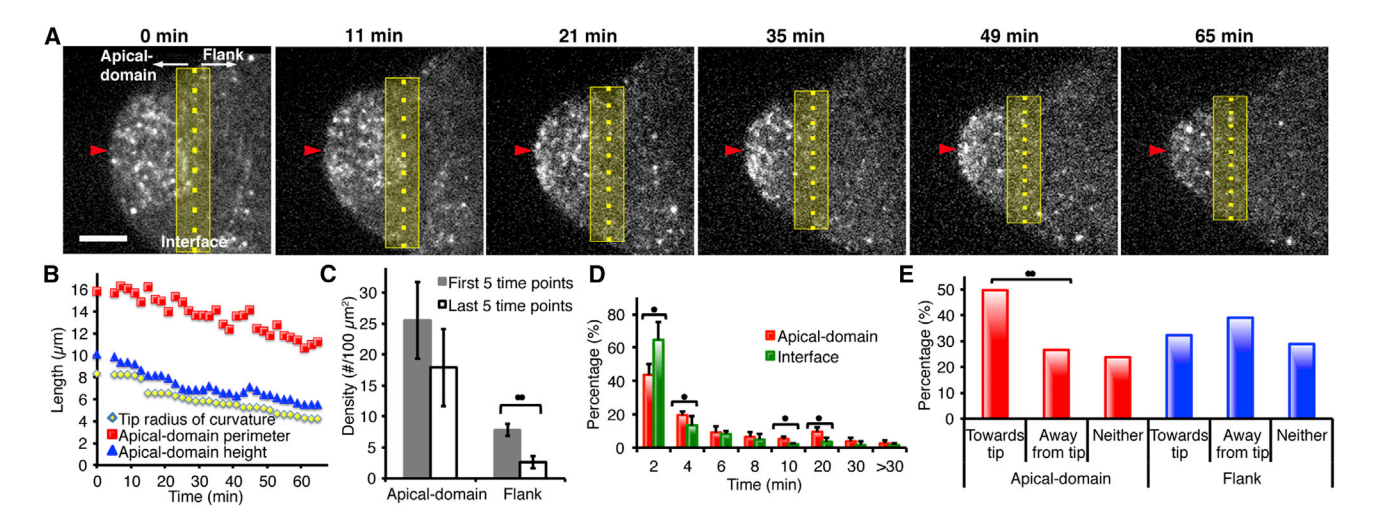


Figure 3. The Lifetime and Direction of Slowly Moving SPK1 Punctae Depend on Their Location within the Cell

- (A) Time-lapsed projected 3D images illustrating the dynamics of SPK1 punctae during cell growth. Red arrowheads, yellow dotted lines, and yellow boxes indicate branch tip, distal boundary of the apical domain, and interface zone, respectively. The scale bar represents 5 μm.
- (B) Quantification of changes in cell shape and the geometry of the apical SPK1 domain during the time course. Size reduction of the SPK1 apical domain is correlated with cell tapering.
- (C) The density of SPK1 punctae is maintained in the apical domain. Mean  $\pm$  SD (n = 5 time points). \*\*p < 0.01 (t test).
- (D) Lifetimes of SPK1 punctae are shorter at the interface of the apical and distal branch domains. Mean ± SD (n = 932 punctae from four cells). \*p < 0.05 (Wilcoxon
- (E) Directional bias of SPK1 punctae movement toward the apex at the extended timescales of branch tapering. Path directionality of SPK1 movement was compared between apical and distal SPK1 punctae (n = 143 in the apical domain and 59 in the flank; \*\*p < 0.01, chi-square test). SPK1 punctae movement in the apical domain was biased toward the branch tip.

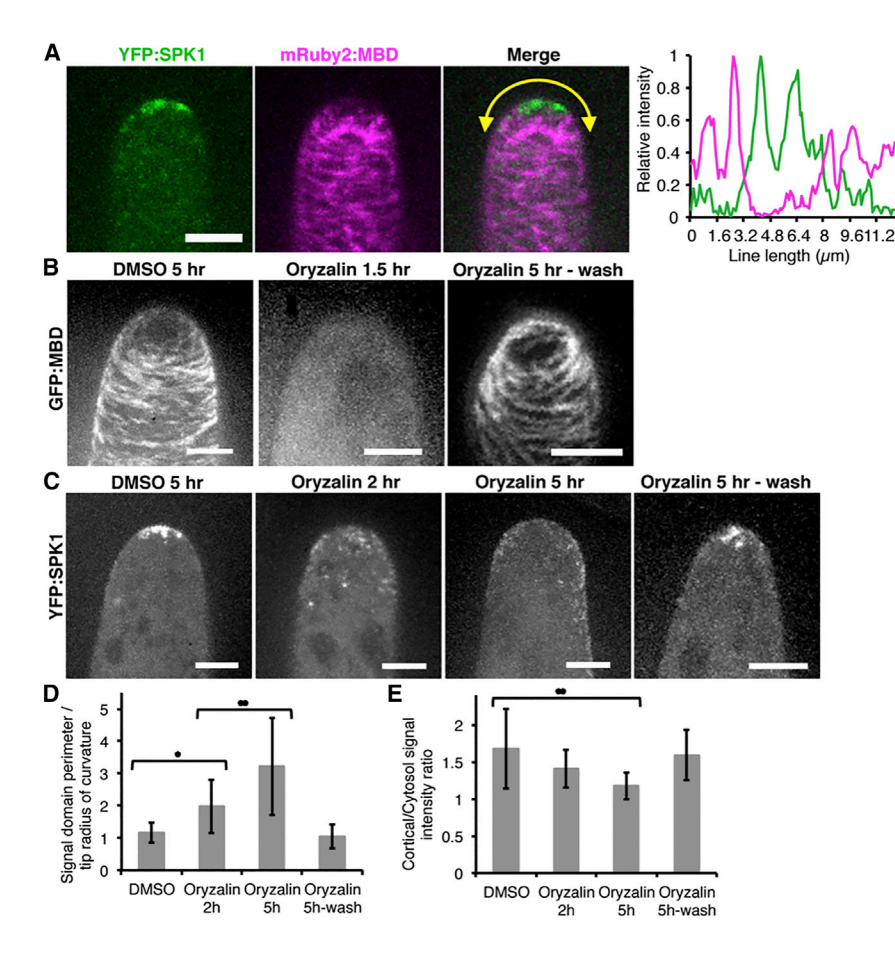
See also Figure S3 and Videos S1 and S2.

for PM-localized proteins [24-26]. In early-stage trichomes, microtubules surround an apical domain where ARP2/3 is activated, and this apical MDZ is a location at which multiple cytoskeletal and cell-wall parameters are integrated to dictate the geometry of cell expansion [6]. We wanted to directly determine whether the SPK1-positive cortical domain resided within the MDZ and whether this localization was influenced by cortical microtubules. Most live-cell probes for microtubules polymerize poorly in young trichomes (Figure S4A). Therefore, we constructed dim trichome-specific mRUBY2:MBD reporter lines that labeled microtubules but did not have a noticeable effect on trichome morphology. Two independent lines were crossed into the YFP:SPK1-expressing line and yielded identical results. Two-color live-cell imaging showed that the cortical domain of SPK1 nodules was always positioned within the apical MDZ (n = 47) (Figure 4A). This result suggests that cortical microtubules influence the distribution of SPK1 signaling nodules at the cell apex.

We next quantified SPK1 localization patterns after treating young trichomes with the microtubule-depolymerizing drug oryzalin, which is known to randomize microtubules and lead to isotropic cell expansion in this cell type [27]. As expected, oryzalin caused isotropic cell swelling (Figure S4B), and its effects on microtubules were reversible (Figures 4B-4E). Following oryzalin treatment, the SPK1 punctae remained associated with the PM, but over time the SPK1-positive cortical domain spread slowly from the apex to more distal regions (Figures 4C, 4D, and S4C). The SPK1-positive cortical domain became progressively dim and the size of individual punctae appeared smaller as the domain spread down the cell flank (Figures 4C-4E). This suggests that the degree of SPK1 clustering is related to the spatial distribution and quality of the endomembrane domain from which they originate. Additional tip-localized parameters are likely to be involved, as SPK1 clustering at the apex as bright and localized SPK1 signals was again detected upon oryzalin removal (Figure 4C). The distribution of BRK1 punctae also progressively broadened in an identical way in response to oryzalin treatment (Figures S4D-S4F). The altered geometries of the BRK1 and SPK1 domains were not driven by changes in cell shape or PM curvature, because the geometry of the cell apex changed very little at the 2 hr and 5 hr time points following oryzalin treatment (Figures 4C and S4D). However, the size of both the SPK1- and BRK1-positive cortical domains became uncoupled from cell shape in the absence of microtubules (Figures S4C and S4E). Because the timescales of the inhibitor treatment exceeded the lifetime of SPK1 nodules by more than an order of magnitude, our results are consistent with a model in which microtubules restrict the distal movement of a specialized PM-anchored organelle system that promotes SPK1-nodule formation. If cortical microtubules simply blocked SPK1 punctae from forming in association with the PM, one would expect new punctae to form anywhere at the cell cortex upon microtubule depolymerization, and that was not observed.

The actin cytoskeleton and acto-myosin transport were not directly required to generate an SPK1 signaling domain, because its localization was not affected even after 3 hr of treatment with the actin-polymerization inhibitor latrunculin B (LatB) (Figures





S4G and S4H). Only after 5 hr of actin depolymerization were there subtle and random effects on the size and location of the SPK1 domain (Figure S4I). We confirmed that 5 hr treatments with LatB do not eliminate the MDZ; instead, its size and position are altered after extended LatB exposure (Figures S4I-S4K). These types of changes in the SPK1 domain are very similar to those reported for arp2/3 mutants that lack an apical actin meshwork but still retain an MDZ, albeit with a more random size and position compared to the wild-type [6]. Together, these results argue against a simple cortical competition model in which cortical actin is required to exclude microtubules from a region of the PM. Instead, the results suggest that the absence of an organized actin cytoskeleton indirectly influences the distributions of the MDZ and SPK1. In arp2/3 mutants the spatial patterns of cell-wall assembly are not properly coordinated with growth [6]. Perhaps the effects of actin depolymerization on SPK1 localization are delayed because its mis-localization is caused by aberrant cell-wall assembly and growth that occur at the timescale of hours. Defective cell-wall mechanical properties could lead to altered feedback between the cell wall and microtubule systems that also disrupts the geometry of the SPK1 domain.

#### **Conclusions**

Specialized cell types assemble spatially distinct actin and microtubule networks to generate predictable shapes [1-3, 28], and in plants cortical actin meshworks within MDZs coordi-

#### Figure 4. Microtubules Confine Signaling Nodules to the Branch Apex

(A) YFP:SPK1 punctae are clustered within a microtubule-depletion zone. Right: representative intensity plot of YFP:SPK1 and mRUBY2:MBD signal along the cell periphery below the yellow

(B) Microtubule organization in developing trichomes expressing GFP:MBD with and without oryzalin treatment. Microtubules are completely depolymerized after ~1.5 hr of orvzalin treatment. but recovered after inhibitor washout.

(C-E) SPK1 localization becomes progressively unfocused following oryzalin treatment, and the effect is reversible following inhibitor washout (C). Perimeter length of the SPK1 signal, normalized by tip radius of curvature, as a function of oryzalin treatment time and inhibitor washout (D). Signal intensity of the cortical SPK1 signal normalized to local cytosolic signal intensity as a function of oryzalin treatment time and inhibitor washout (E). Mean  $\pm$  SD (n = 22). \*p < 0.05, \*\*p < 0.01 (ANOVA with Tukey HSD test).

Scale bars represent 5  $\mu m$ . See also Figure S4.

nate long-distance transport and cellwall assembly to pattern growth at the cellular scale [1, 5, 6]. Here, we show that a broad apical zone of microtubule depletion is a cellular hub for cellshape control where the ROP GEF SPK1 is a permanent resident. When fully activated, SPK1 recruits W/SRC to a

distributed network of PM-associated organelle domains, and the resulting ARP2/3-dependent actin meshwork organizes cytoplasmic flow that has been shown to maintain cell-wall thickness gradients that enable polarized growth cellular scales [6]. Activating SPK1 signals are transmitted from a concentrated population of unstable nodules that appear to be physically linked to the PM. Importantly, the network of SPK1 nodules is confined to the cell apex by a negative feedback loop in which cortical microtubules restrict the movement of the SPK1 punctae. Septins have a general role as diffusion barriers to confine signaling molecules to a specific subcellular domain [29]. However, septins are absent in plants, and we show here that microtubules most likely provide a similar function to confine SPK1 signaling within the MDZ boundary. During cell tapering, there are additional forms of feedback control in which the geometry of the ARP2/3 complex activation domain is adaptively tuned to a decreasing cell radius of curvature, and this feedback may occur at the MDZ boundary, where wall stress is maximal and microtubules are stabilized [6]. We propose that the slow process of actin-dependent secretion and cell-wall assembly enables accurate information flow between the cell wall and the MDZ. We anticipate this new knowledge about the cellular-scale controls of actin, microtubules, and morphogenesis will serve as a useful comparative model for other cell types that use a diffuse growth mechanism, and accelerate the engineering of improved traits for economically important plant cell types such as cotton fibers.



#### **STAR**\*METHODS

Detailed methods are provided in the online version of this paper and include the following:

- KEY RESOURCES TABLE
- CONTACT FOR REAGENT AND RESOURCE SHARING
- EXPERIMENTAL MODEL AND SUBJECT DETAILS
- METHOD DETAILS
  - O Plasmid constructs and transgenic lines
  - YFP:SPK1 rescue analysis
  - Confocal fluorescent microscopy
  - O Measurements of tip radius of curvature and signal domain perimeter
  - O FM4-64 staining and peak intensity analysis
  - O SPK1 punctae: size and density analysis
  - O Particle tracking analysis
  - Cytoskeleton inhibitor analysis
- QUANTIFICATION AND STATISTICAL ANALYSIS

#### **SUPPLEMENTAL INFORMATION**

Supplemental Information includes four figures, two tables, and two videos and can be found with this article online at https://doi.org/10.1016/j.cub. 2018.05.076.

#### **ACKNOWLEDGMENTS**

We thank Eileen Mallery, Albert Fenton, and Nita Basu for assistance in creating the CRIB:GFP line. We would like to thank Richard Cyr and David Marks for the gift of the MBD2 and MYB5 promoter clones that Eileen Mallery used to construct and validate the mRUBY2:GFP line. We would like to thank Laurie Smith, Federica Brandizzi, Abel Rosado, and Patrick Hussey for making their reporter strains available to us. This work was supported by NSF MCB grant 1121893 (to D.B.S.).

#### **AUTHOR CONTRIBUTIONS**

 $\mbox{M.Y.}$  and  $\mbox{D.B.S.}$  conceived the experiments.  $\mbox{M.Y.}$  conducted the experiments and analyzed the data. J.M.A. helped to create the recombineering tools. M.Y., D.B.S., and J.M.A. wrote the paper.

#### **DECLARATION OF INTERESTS**

The authors declare no competing interests.

Received: March 5, 2018 Revised: April 23, 2018 Accepted: May 24, 2018 Published: July 19, 2018

#### **REFERENCES**

- 1. Panteris, E., and Galatis, B. (2005). The morphogenesis of lobed plant cells in the mesophyll and epidermis: organization and distinct roles of cortical microtubules and actin filaments. New Phytol. 167, 721-732.
- 2. Murphy, D.A., and Courtneidge, S.A. (2011). The 'ins' and 'outs' of podosomes and invadopodia: characteristics, formation and function. Nat. Rev. Mol. Cell Biol. 12, 413-426.
- 3. Coles, C.H., and Bradke, F. (2015). Coordinating neuronal actin-microtubule dynamics. Curr. Biol. 25, R677-R691.
- 4. Baskin, T.I. (2005). Anisotropic expansion of the plant cell wall. Annu. Rev. Cell Dev. Biol. 21, 203-222

- 5. Szymanski, D.B. (2009). Plant cells taking shape: new insights into cytoplasmic control. Curr. Opin. Plant Biol. 12, 735-744.
- 6. Yanagisawa, M., Desyatova, A.S., Belteton, S.A., Mallery, E.L., Turner, J.A., and Szymanski, D.B. (2015). Patterning mechanisms of cytoskeletal and cell wall systems during leaf trichome morphogenesis. Nat. Plant 1,
- 7. Xu, T., Wen, M., Nagawa, S., Fu, Y., Chen, J.G., Wu, M.J., Perrot-Rechenmann, C., Friml, J., Jones, A.M., and Yang, Z. (2010). Cell surfaceand Rho GTPase-based auxin signaling controls cellular interdigitation in Arabidopsis. Cell 143, 99-110.
- 8. Basu, D., Le, J., Zakharova, T., Mallery, E.L., and Szymanski, D.B. (2008). A SPIKE1 signaling complex controls actin-dependent cell morphogenesis through the heteromeric WAVE and ARP2/3 complexes. Proc. Natl. Acad. Sci. USA 105, 4044-4049.
- 9. Qiu, J.L., Jilk, R., Marks, M.D., and Szymanski, D.B. (2002). The Arabidopsis SPIKE1 gene is required for normal cell shape control and tissue development. Plant Cell 14, 101-118.
- 10. Stradal, T.E., and Scita, G. (2006). Protein complexes regulating Arp2/ 3-mediated actin assembly. Curr. Opin. Cell Biol. 18, 4-10.
- 11. Zhang, C., Mallery, E.L., Schlueter, J., Huang, S., Fan, Y., Brankle, S., Staiger, C.J., and Szymanski, D.B. (2008). Arabidopsis SCARs function interchangeably to meet actin-related protein 2/3 activation thresholds during morphogenesis. Plant Cell 20, 995-1011.
- 12. Yanagisawa, M., Zhang, C., and Szymanski, D.B. (2013). ARP2/3-dependent growth in the plant kingdom: SCARs for life. Front. Plant Sci. 4, 166.
- 13. Uhrig, J.F., Mutondo, M., Zimmermann, I., Deeks, M.J., Machesky, L.M., Thomas, P., Uhrig, S., Rambke, C., Hussey, P.J., and Hülskamp, M. (2007). The role of Arabidopsis SCAR genes in ARP2-ARP3-dependent cell morphogenesis. Development 134, 967-977.
- 14. Zhou, R., Benavente, L.M., Stepanova, A.N., and Alonso, J.M. (2011). A recombineering-based gene tagging system for Arabidopsis. Plant J. 66, 712-723
- 15. Berken, A., Thomas, C., and Wittinghofer, A. (2005). A new family of RhoGEFs activates the Rop molecular switch in plants. Nature 436,
- 16. Le, J., Mallery, E.L., Zhang, C., Brankle, S., and Szymanski, D.B. (2006). Arabidopsis BRICK1/HSPC300 is an essential WAVE-complex subunit that selectively stabilizes the Arp2/3 activator SCAR2. Curr. Biol. 16,
- 17. Djakovic, S., Dyachok, J., Burke, M., Frank, M.J., and Smith, L.G. (2006). BRICK1/HSPC300 functions with SCAR and the ARP2/3 complex to regulate epidermal cell shape in Arabidopsis. Development 133, 1091–1100.
- 18. Dyachok, J., Shao, M.R., Vaughn, K., Bowling, A., Facette, M., Djakovic, S., Clark, L., and Smith, L. (2008). Plasma membrane-associated SCAR complex subunits promote cortical F-actin accumulation and normal growth characteristics in Arabidopsis roots. Mol. Plant 1, 990-1006.
- 19. Perroud, P.F., and Quatrano, R.S. (2008). BRICK1 is required for apical cell growth in filaments of the moss Physcomitrella patens but not for gametophore morphology. Plant Cell 20, 411-422.
- 20. Kunisaki, Y., Nishikimi, A., Tanaka, Y., Takii, R., Noda, M., Inayoshi, A., Watanabe, K., Sanematsu, F., Sasazuki, T., Sasaki, T., and Fukui, Y. (2006). DOCK2 is a Rac activator that regulates motility and polarity during neutrophil chemotaxis. J. Cell Biol. 174, 647-652.
- 21. Zhang, C., Kotchoni, S.O., Samuels, A.L., and Szymanski, D.B. (2010). SPIKE1 signals originate from and assemble specialized domains of the endoplasmic reticulum. Curr. Biol. 20, 2144-2149.
- 22. Zhang, C., Mallery, E., Reagan, S., Boyko, V.P., Kotchoni, S.O., and Szymanski, D.B. (2013). The endoplasmic reticulum is a reservoir for WAVE/SCAR regulatory complex signaling in the Arabidopsis leaf. Plant Physiol. 162, 689-706.
- 23. Ambrose, J.C., Shoji, T., Kotzer, A.M., Pighin, J.A., and Wasteneys, G.O. (2007). The Arabidopsis CLASP gene encodes a microtubule-associated protein involved in cell expansion and division. Plant Cell 19, 2763-2775.

Please cite this article in press as: Yanagisawa et al., Microtubule-Dependent Confinement of a Cell Signaling and Actin Polymerization Control Module Regulates Polarized Cell Growth, Current Biology (2018), https://doi.org/10.1016/j.cub.2018.05.076



- 24. Paredez, A.R., Somerville, C.R., and Ehrhardt, D.W. (2006). Visualization of cellulose synthase demonstrates functional association with microtubules. Science 312, 1491-1495.
- 25. Oda, Y., and Fukuda, H. (2012). Initiation of cell wall pattern by a Rho- and microtubule-driven symmetry breaking. Science 337, 1333-1336.
- 26. Sugiyama, Y., Wakazaki, M., Toyooka, K., Fukuda, H., and Oda, Y. (2017). A novel plasma membrane-anchored protein regulates xylem cell-wall deposition through microtubule-dependent lateral inhibition of Rho GTPase domains. Curr. Biol. 27, 2522-2528.e4.
- 27. Szymanski, D.B., Marks, M.D., and Wick, S.M. (1999). Organized F-actin is essential for normal trichome morphogenesis in Arabidopsis. Plant Cell 11, 2331-2347.
- 28. Kobayashi, H., Fukuda, H., and Shibaoka, H. (1988). Interrelation between the spatial disposition of actin filaments and microtubules during the differentiation of tracheary elements in cultured Zinnia cells. Protoplasma 143 29-37
- 29. Mostowy, S., and Cossart, P. (2012). Septins: the fourth component of the cytoskeleton. Nat. Rev. Mol. Cell Biol. 13, 183-194.
- 30. Sharan, S.K., Thomason, L.C., Kuznetsov, S.G., and Court, D.L. (2009). Recombineering: a homologous recombination-based method of genetic engineering. Nat. Protoc. 4, 206-223.

- 31. El-Assal, S.E.-D., Le, J., Basu, D., Mallery, E.L., and Szymanski, D.B. (2004). DISTORTED2 encodes an ARPC2 subunit of the putative Arabidopsis ARP2/3 complex. Plant J. 38, 526-538.
- 32. Basu, D., El-Assal, S.E.-D., Le, J., Mallery, E.L., and Szymanski, D.B. (2004). Interchangeable functions of Arabidopsis PIROGI and the human WAVE complex subunit SRA1 during leaf epidermal development. Development 131, 4345-4355.
- 33. Gutierrez, R., Lindeboom, J.J., Paredez, A.R., Emons, A.M., and Ehrhardt, D.W. (2009). Arabidopsis cortical microtubules position cellulose synthase delivery to the plasma membrane and interact with cellulose synthase trafficking compartments. Nat. Cell Biol. 11, 797-806.
- 34. Vermeer, J.E., van Leeuwen, W., Tobeña-Santamaria, R., Laxalt, A.M., Jones, D.R., Divecha, N., Gadella, T.W., Jr., and Munnik, T. (2006). Visualization of Ptdlns3P dynamics in living plant cells. Plant J. 47,
- 35. Nelson, B.K., Cai, X., and Nebenführ, A. (2007). A multicolored set of in vivo organelle markers for co-localization studies in Arabidopsis and other plants. Plant J. 51, 1126-1136.
- 36. Marc, J., Granger, C.L., Brincat, J., Fisher, D.D., Kao, T.-h., McCubbin, A.G., and Cyr, R.J. (1998). A GFP-MAP4 reporter gene for visualizing cortical microtubule rearrangements in living epidermal cells. Plant Cell 10, 1927-1940.



### **STAR**\***METHODS**

#### **KEY RESOURCES TABLE**

REAGENT or RESOURCE	SOURCE	IDENTIFIER
Bacterial and Virus Strains		
E. coli SW105	[30]	N/A
Chemicals, Peptides, and Recombinant Proteins		
-M4-64	Invitrogen	Cat # T3166
MitoTracker Red CMXRos	ThermoFisher	Cat # M7512
Oryzalin	Dow AgroSciences	CAS 19044-88-3
atrunculin B	Sigma-Aldrich	CAS 76343-94-7
Experimental Models: Organisms/Strains		
Arabidopsis: spk1-1	[9]	N/A
Arabidopsis: arpc2/dis2-1	[31]	N/A
Arabidopsis: sra1/pir-3	[32]	N/A
Arabidopsis: BRK1:YFP	L. Smith	N/A
Arabidopsis: YFP:CESA6	[33]	N/A
Arabidopsis: YFP:2xFYVE	[34]	N/A
Arabidopsis: CFP:PTS1	[35]	N/A
Arabidopsis: YFP:SEC24A	F. Brandizzi	N/A
Arabidopsis: SYT1:GFP	A. Rosado	N/A
Arabidopsis: VAP27:GFP	PJ. Hussey	N/A
Arabidopsis: GFP:MBD	[36]	N/A
Arabidopsis: ARP2/3:GFP	[6]	N/A
Arabidopsis: YFP:SPK1	This study	N/A
Arabidopsis: CRIB:GFP	This study	N/A
Arabidopsis: YFP:SPK1; mRUBY:MBD	This study	N/A
Arabidopsis: YFP:SPK1; LifeAct:mCherry	This study	N/A
Digonucleotides	•	
SPK1_REC_N_F: CTCTCTAATGGCGTAGTAGTACCTCACA	This study	N/A
SPK1_REC_N_R: AGAGGCTGACGAGGTAGCTTACGAAAT CGAAGACCAAGATTGTTGTTCTCGGCCCCAGCGGCCGC AGCAGCACC	This study	N/A
RIC1p2-Fnew: CACCTCTAGAATGGCGACGACAATGAAGG	This study	N/A
RIC1p2-Rnew: AAGCTTCTACCCTTGCGGGTTGTATTTG	This study	N/A
FMYB5: cgccaagcttctagagagctctgctggagaaattcatcccaa	This study	N/A
PR_MYB5mRUBY2: GATTAACTCCTCTCCTTTGGACACC ATggtggcgaccggtct	This study	N/A
BF_MYB5mRUBY2: agaccggtcgccaccATGGTGTCCAAAG GAGAGGAGTTAATC	This study	N/A
BR_mRUBY2MBD: cctttgcttcttcttgccgggaCTTATACAATT	This study	N/A
F_mRUBY2MBD: GGCGGTGGTATGGATGAATTGTAT AGtcccggcaagaagaagcaaag	This study	N/A
	This study	N/A
IR_nosT_EcoRI: cgacggccagtgaattctcatgt	This study	
R_nosT_EcoRI: cgacggccagtgaattctcatgt	This study	
	[14]	N/A
Recombinant DNA	,	

(Continued on next page)



Continued			
REAGENT or RESOURCE	SOURCE	IDENTIFIER	
pGWB6	T. Nakagawa	N/A	
GFP:MBD	[36]	N/A	
pEGADMYB5	D. Marks	N/A	
pFA6a-link-yomRuby2-Kan	Addgene	Cat # 44953	
pENTR/D/TOPO	Invitrogen	Cat # K240020	
CRIBpENT	This study	N/A	
CRIBpGWB6	This study	N/A	
pENT:mRUBY2:MBD	This study	N/A	
pCB302:mRUBY2:MBD	This study	N/A	
Software and Algorithms			
ImageJ	NIH	http://imagej.nih.gov/ij/	
SlideBook 6.0	Intelligent Imaging Innovations	https://www.intelligent-imaging.com/ slidebook	
Excel	Microsoft	N/A	
R	N/A	https://www.r-project.org/	
Photoshop CS5	Adobe	N/A	

#### CONTACT FOR REAGENT AND RESOURCE SHARING

Further information and requests for resources and reagents should be directed to and will be fulfilled by the lead contact, Dan Szymanski (szymandb@purdue.edu).

#### **EXPERIMENTAL MODEL AND SUBJECT DETAILS**

Arabidopsis thaliana ecotype Columbia (Col) was used as the wild-type in this study. Mutant alleles and transgenic lines are listed in the Key Resources Table. For fluorescence imaging, plants were grown on half-strength Murashige and Skoog media containing 1% sucrose and 0.5 or 0.8% agar under continuous light (110 μmol m<sup>-2</sup> sec<sup>-1</sup>) at 22°C. In this study, all developing trichomes are defined as stage 4 trichomes with blunt tips and branch length less than 50 µm. For spk1 mutant trichomes that are often unbranched. Therefore it was not possible to distinguish between a stalk and a branch, and trichomes with total length less than 120 µm were similar in total length to equivalent to stage 4 wild-type cells.

#### **METHOD DETAILS**

#### Plasmid constructs and transgenic lines

To generate YFP:SPK1, a 3xYpet tag was fused to the N terminus of SPK1 by recombineering [14]. Recombineering primers were designed as following: the forward primer contains 50 nucleotides ending the start codon of the SPK1 gene sequence and 18 nucleotides from the 5' end of the 3xYpet cassette; the reverse primer contains 50 nucleotides right after the start codon of the SPK1 gene sequence and 24 nucleotides from the 3' end of the 3xYpet cassette (see Key Resources Table for sequences). The SPK1-3xYpet recombineering cassette was generated by PCR amplification of the 3xYpet cassette using the recombineering primers. The JAtY68D18 clone was transformed into the recombineering competent E.coli strain SW105 and recombined with the SPK1-3xYpet recombineering cassette. The 3xYpet tagged clone was transformed into Agrobacterium and then into SPK1/spk1-1 plants. Homozygous lines for both YFP:SPK1 and spk1-1 T-DNA were obtained from the T2 generation and used in this study.

For generation of CRIB:GFP, the CRIB domain of RIC1 was PCR amplified from Arabidopsis EST RZ03E09R (Kazusa, Japan) and cloned into the Gateway vector pENTR/D/TOPO (Invitrogen, Carlsbad, CA). The CRIBpENT plasmid was sequence verified and recombined into the pGWB6 binary vector (provided by T. Nakagawa, Shimane University, Japan). The resulting plasmid CRIBpGWB6 was introduced into Arabidopsis by Agrobacterium-mediated transformation and lines were selected that had no detectable effect on whole plant or trichome morphology.

mRUBY2:MBD was created by a 2-step overlap PCR reaction. The MYB5 promoter, mRUBY2 and MBD-nos terminator were amplified from pEGADMYB5pro (provided by D Marks, University of Minnesota, St. Paul, MN), pFA6a-link-yomRuby2-Kan (Addgene, Cambridge, MA) and GFP:MBD [36], respectively. The resulting 3.6 kb fragment harboring Xbal and EcoRl restriction sites was cloned into pENTR/D/TOPO for sequencing. The MYB5p:mRUBY2:MBD:nosT sequence was digested and cloned into the pCB302 binary vector for Agrobacterium-mediated plant transformation.



ARP2/3:GFP has been previously described [6]. BRK1:YFP, YFP:SEC24A, SYT1:GFP and VAP27:GFP seeds were provided by L. Smith (University of California, San Diego, CA), F. Brandizzi (Michigan State University, East Lansing, MI), A. Rosado (University of British Columbia, Vancouver, BC) and PJ. Hussey (Durham University, Durham, UK), respectively. All other lines used in this study were generated by crossing.

#### YFP:SPK1 rescue analysis

T1 generations of YFP:SPK1 transgenic lines were obtained by *Agrobacterium*-mediated transformation into SPK1-1/spk1-1 heterozygous plants. T1 seeds were screened for Basta resistance on 1/2 MS plates containing 1:50,000 (10  $\mu$ g/mL) Basta. Transformation of the entire construct was rare, and was confirmed by genotyping of SacB gene, which is located next to the T-DNA right border. Transformants harboring the *spk1-1* T-DNA with a kanamycin resistant gene were selected for the rescue analysis. T2 seeds were grown on 1/2 MS plates containing 50  $\mu$ g/mL Kanamycin to see segregation ratio for *spk1* and wild-type phenotypes. The tests of phenotypic rescue were performed using a chi-square test using a null hypothesis in which the YFP:SPK1 construct does not rescue *spk1* mutant, and therefore segregation ratio of mutant and wild-type phenotype would be 1:2 on a kanamycin plate because SPK1-1/SPK1-1 plants are dead.

#### **Confocal fluorescent microscopy**

Fluorescent images were detected using a Photometrix Evolve 512 (Tuscon, Az) intensified CCD camera acquired using a CSU-X1 spinning disk confocal head (Yokogawa Electric Corporation, Tokyo, Japan) mounted on a Zeiss Observer.Z1 inverted microscope with a 60X C-Apo 1.2 NA water-immersion objective or a 100X PlanApo 1.46 NA oil-immersion objective to quantify individual punctae. Image processing and quantification were performed using ImageJ (http://imagej.nih.gov/ij/) and SlideBook version 6.0 (Intelligent Imaging Innovations, Denver, CO). Images were edited using Photoshop CS5 (Adobe) for data presentation.

#### Measurements of tip radius of curvature and signal domain perimeter

Tip radius of curvature is the radius of the circle that best fits the cell wall perimeter of branch tip. Apical domain perimeter was measured by drawing a segmented line along the perimeter of branch tip where signal is clearly present above background.

#### FM4-64 staining and peak intensity analysis

Whole seedlings at 10 to 13 DAG expressing YFP:SPK1 or BRK1:YFP were stained with 1  $\mu$ M FM4-64 for 2 hr or longer. Fluorescence signals from FM4-64 and YFP in trichome branches were captured by sequential excitations by 561 and 515 lasers, respectively. A single optical section showing a mid-plane of branches was selected from z stack images for colocalization analysis. Signal intensity was measured along 3-pixel lines by Plot Profile function in ImageJ and robust profiles were analyzed. Relative intensity was determined by the equation:

$$(X_{intensity} - Min_{intensity}) / (Max_{intensity} - Min_{intensity})$$

#### SPK1 punctae: size and density analysis

Maximum intensity projections were used to determine size and density of SPK1 punctae. Images were band-pass filtered with a 1-2.5 pixel setting using the Filter2D plugin (https://lpixel.net/en/services/lpixel-imagej-plugins/) to reduce noise, and then thresholded to make binary images. The Analyze Particles function in ImageJ was used to obtain size and numbers of punctae.

#### Particle tracking analysis

Confocal image stacks of trichome branches expressing YFP:SPK1 were captured for 1-2 hr with 1 or 2 min intervals. Maximum intensity projections from different time points were stacked to create a 3D time-lapse image. A 10  $\mu$ m line was drawn horizontally from the externe branch apex into the cell in each time point, and then images were aligned by the Align image by line ROI function in ImageJ. The aligned image stack was processed using a 2D Laplacian filter to enhance signal to noise ratios, and then thresholded to create a segment mask. Identified particles were tracked using the Particle Tracking Protocol function in the SlideBook software. The tracked particles were categorized into three populations based on their initial location: apical-domain, flank and interface. The interface was defined as an area within 2  $\mu$ m from the outer boundary of apical-domain. To determine directionality, initial and final distance from the reference tip point was calculated for each particle, and then a direction relative to tip was determined by subtracting initial distance from final distance. The particles with subtracted value less than one pixel were categorized in the "Neither" population.

#### Cytoskeleton inhibitor analysis

 $A\,2\,\mu\text{L-drop}$  of 100  $\mu\text{M}$  oryzalin (Dow AgroSciences, Indianapolis, IN) was applied on the shoot meristem and emerging leaves of 10 to 13 DAG seedlings expressing GFP:MBD [36], BRK1:YFP, or YFP:SPK1. To wash out oryzalin, seedlings were incubated in a 0.4 M

Please cite this article in press as: Yanagisawa et al., Microtubule-Dependent Confinement of a Cell Signaling and Actin Polymerization Control Module Regulates Polarized Cell Growth, Current Biology (2018), https://doi.org/10.1016/j.cub.2018.05.076



mannitol solution for 20 min x 3. The washed seedlings were rinsed with water and placed on an MS agar plate overnight. For actin depolymerizing experiments, 5-10 µL of 2 µM latrunculin B (Sigma-Aldrich, St. Louis, MO) was applied to each seedling expressing GFP:MBD or YFP:SPK1 and LifeAct:mCherry.

#### **QUANTIFICATION AND STATISTICAL ANALYSIS**

Statistical analyses were performed using R for Shapiro-Wilk normality test, Wilcoxson test, ANOVA and Tukey HSD test and Microsoft Excel for t test and chi-square test. Type of statistical tests and error bars, sample size, and significances are shown in the figure legends.

**Current Biology, Volume 28** 

# **Supplemental Information**

Microtubule-Dependent Confinement
of a Cell Signaling and Actin Polymerization
Control Module Regulates Polarized Cell Growth

Makoto Yanagisawa, Jose M. Alonso, and Daniel B. Szymanski

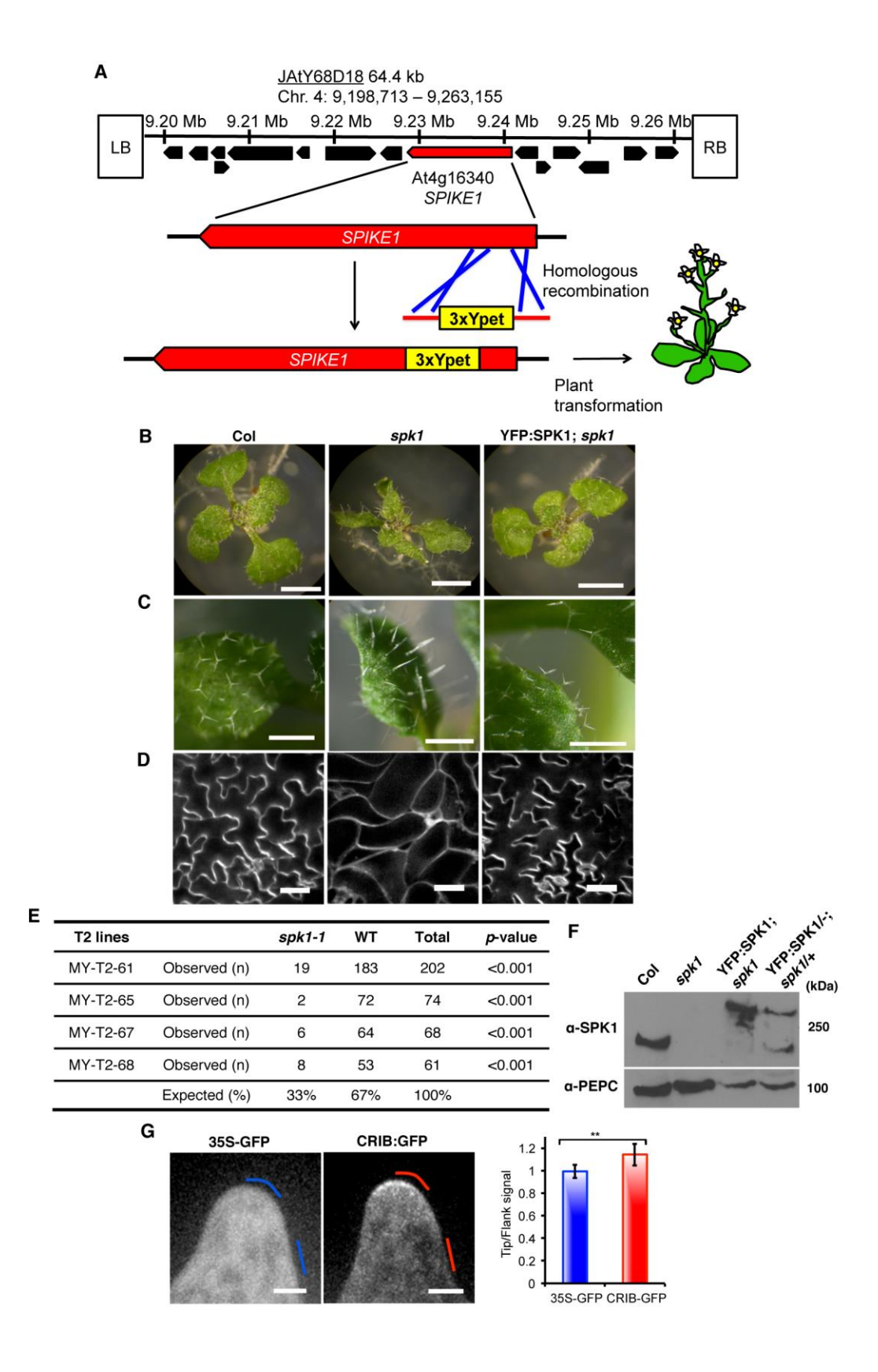


Figure S1. Live-cell probe validation for SPK1 and active ROPs, Related to Figure 1.

(A) The N-terminus of SPK1 was tagged with 3xYpet (YFP) by homologous recombination in the JAtY clone 68D18. (B) Leaf morphology of 12 days after germination (DAG) seedlings. Scale bars represent 2 mm. (C) Leaf trichome morphology. Scale bars represent 1 mm. (D) Pavement cell shapes defined by propidium iodide staining of 12 DAG cotyledons. Scale bars represent 50  $\mu$ m. (E) YFP:SPK1 rescue analysis by a chi-square test. (F) Proteins from wild type, spk1, YFP:SPK1/spk1 homozygous and heterozygous lines were probed with anti-SPK1 antibody. PEPC was used as loading control. YFP:SPK1 in YFP:SPK1; spk1+ plants was tip localized in trichomes similar to Figure 1C. (G) Signal intensities at the tip (upper lines) and flank (lower lines) regions in trichome branches expressing 35S-GFP (left panel) and CRIB:GFP (middle panel) were measured. Scale bars represent 5  $\mu$ m. The tip/flank ratio of the total integrated intensity at the two cellular locales is shown in the right panel. Mean  $\pm$  SD (n = 20). \*\*P < 0.01 (t = 10).

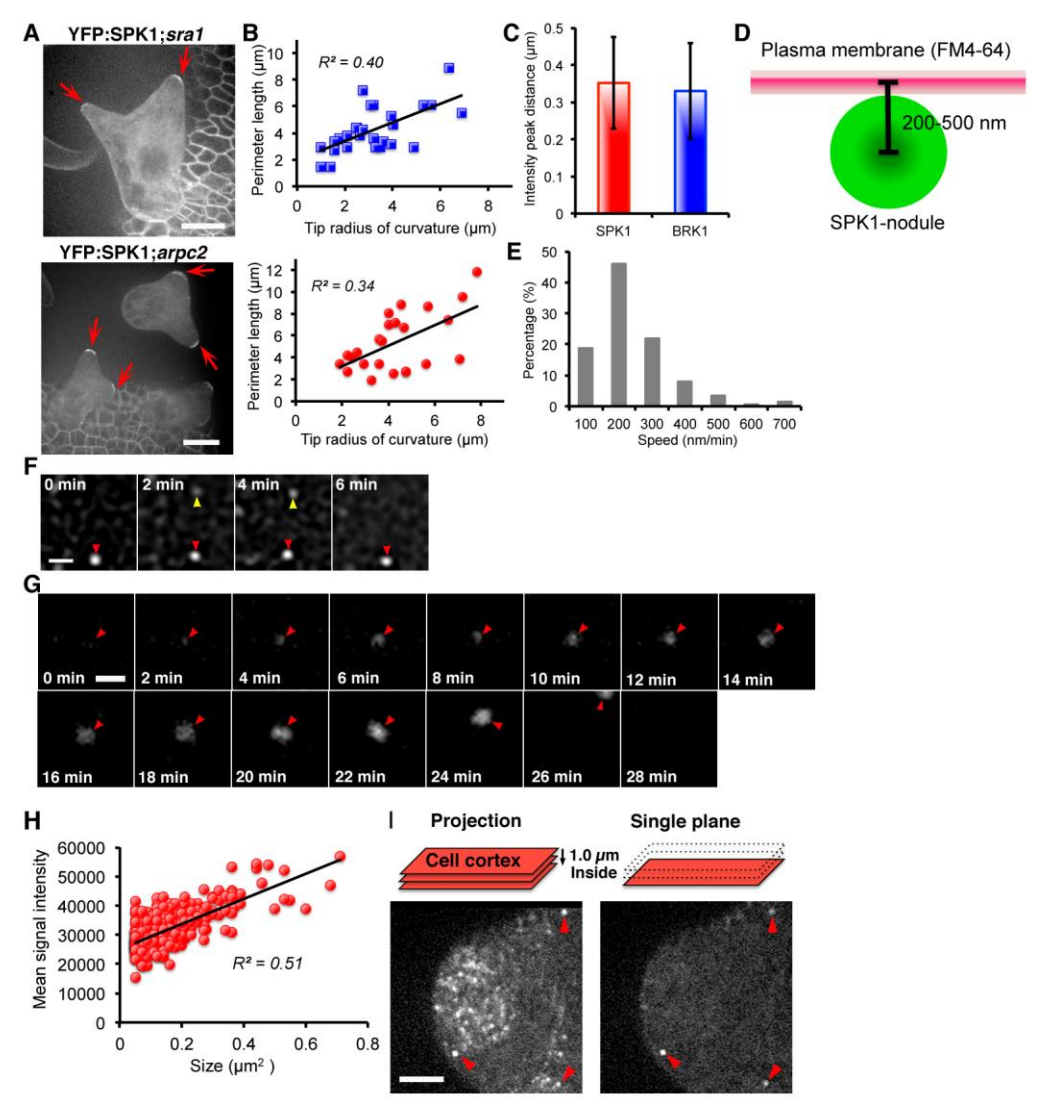


Figure S2. SPK1 localization in the absence of W/SRC and ARP2/3 subunits, and particle tracking of SPK1-positive punctae, Related to Figure 2.

(A and B) SPK1 localization in the absence of W/SRC and ARP2/3 subunits. Polarized accumulation of SPK1 was not altered in sra1 and arpc2 developing trichomes (A). Scale bars represent 20 µm. However, correlations between the size of the SPK1 signaling domain and cell geometry were disrupted (B). (C) Distinct separations of the plasma membrane (FM4-64) and YFP:SPK1 and BRK1:YFP intensity peaks at the cell apex of trichomes. Mean  $\pm$  SD (n > 10). Intensity peaks of both YFP:SPK and BRK1:YFP were proximal to those of FM4-64 with mean distances of 0.35 and 0.33 µm, respectively. (D) The distance of intensity peaks between FM4-64 and SPK1-nodule largely depend on size of SPK1-nodule. Plasma membrane appears thick in Figure 2F and 2H because the image resolution (Airy radius) for FM4-64 is 234 nm. (E) Frequency distribution of SPK1 puntae speeds taken from multiple time lapse imaging experiments. Mean speed is  $228 \pm 156$  nm/min (n = 279 punctae in 2 cells). (F and G) Examples of individual SPK1 punctae behaviors at the cell cortex. Scale bars represent 1 µm in (F) and 0.5 um in (G), (G) SPK1 clustering and detachment in a large punctae. At 22 min the SPK1 punctae in panel G becomes subcortical and streams out of the imaging volume soon thereafter. (H) Scatter plot of mean pixel intensity as a function of SPK1 punctae size, indicating a greater number of SPK1 molecules within larger SPK1 punctae. (I) Example image of rare cytosolic punctae. Scale bar represents 5 µm.

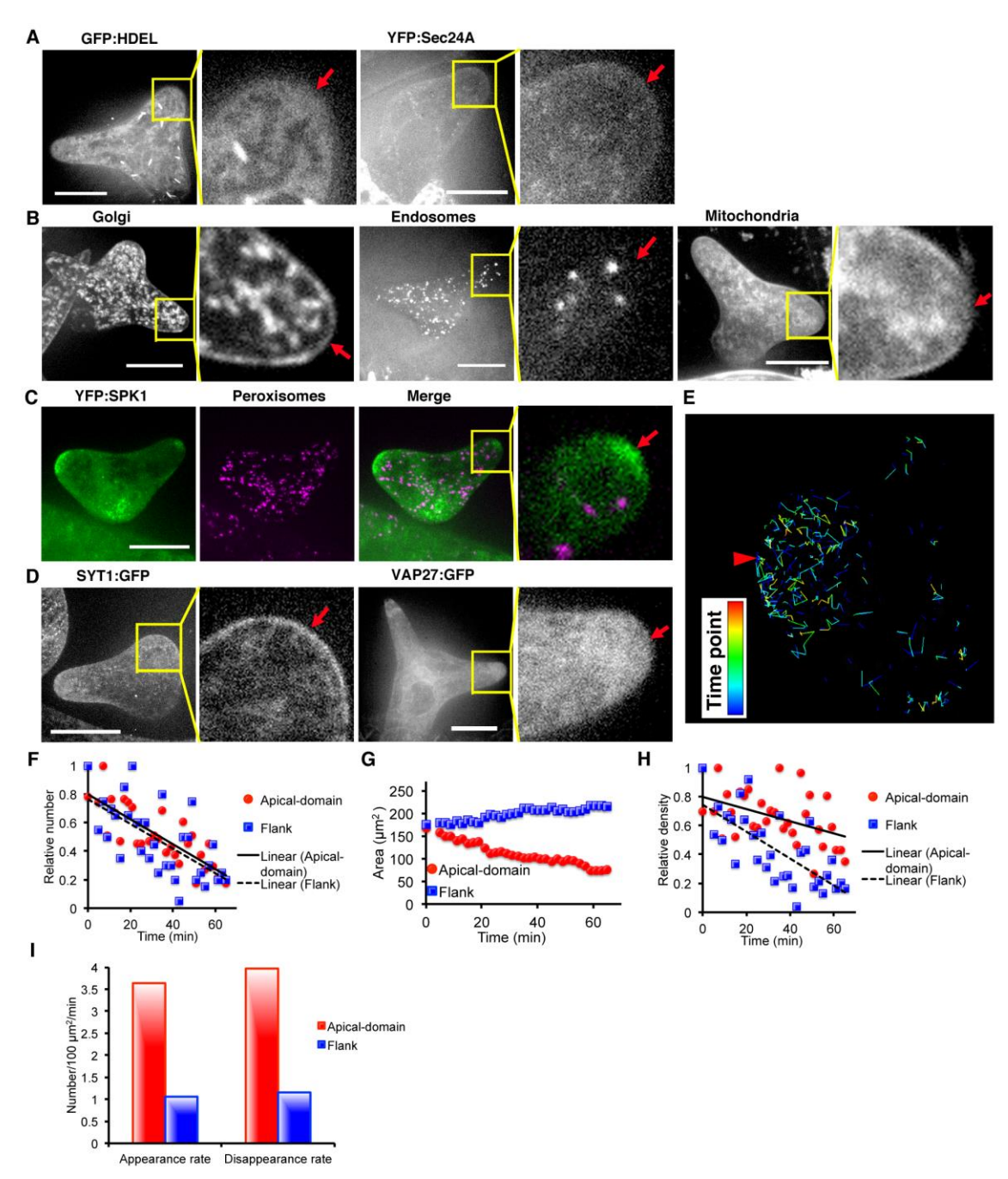


Figure S3. Localization of several organelles in relation to SPK1 punctae in young stage trichomes, and analysis of SPK1 punctae stability and movement as a function of location, Related to Figures 2 and 3.

(A-D) Representative localization images of major organelles in developing trichomes. Magnified mid-plane images of branch tips enclosed by yellow lines are shown in the right panels. Arrows mark the extreme branch apex. Scale bars represent 20 μm. Localization of the bulk ER maker GFP:HDEL and the ER exit site marker SEC24A (A). Golgi, endosomes and mitochondria were visualized by YFP:CESA6 [S1], YFP:2xFYVE [S2] and MitoTracker (ThermoFisher), respectively (B). None of these were concentrated at the branch apex, and all displayed vigorous cytoplasmic steaming. Vacuoles are excluded from the branch apex at this developmental stage [S3]. Localization of SPK1 and peroxisomes (C). CFP:PTS1 [S4] was used to detect peroxisomes.

Known ER-plasma-membrane contact site markers SYT1 and VAP27 in developing trichomes had a broad localization pattern but were often concentrated at the branch apex (D). (E) Maximum projection of tracks in all time frames after particle tracking (from the cell shown in Figure 3A). (F) Quantification of SPK1 punctae number as a function of time in the apical domain and flanking region of developing trichomes. The number of punctae was normalized from 0 to 1 based on minimum and maximum numbers within time lapse experiments to allow them to be pooled. (G) Measurement of the cross sectional area of the apical domain and the flank, indicating that the apical domain becomes smaller and the flank expands as the branch elongates. (H) The density of SPK1 punctae is relatively constant in the apical domain, and becomes progressively less dense in the flanking region of elongating branches. (I) SPK1 punctae form 3.5 times more frequently in the apical domain compared to the flanking region.

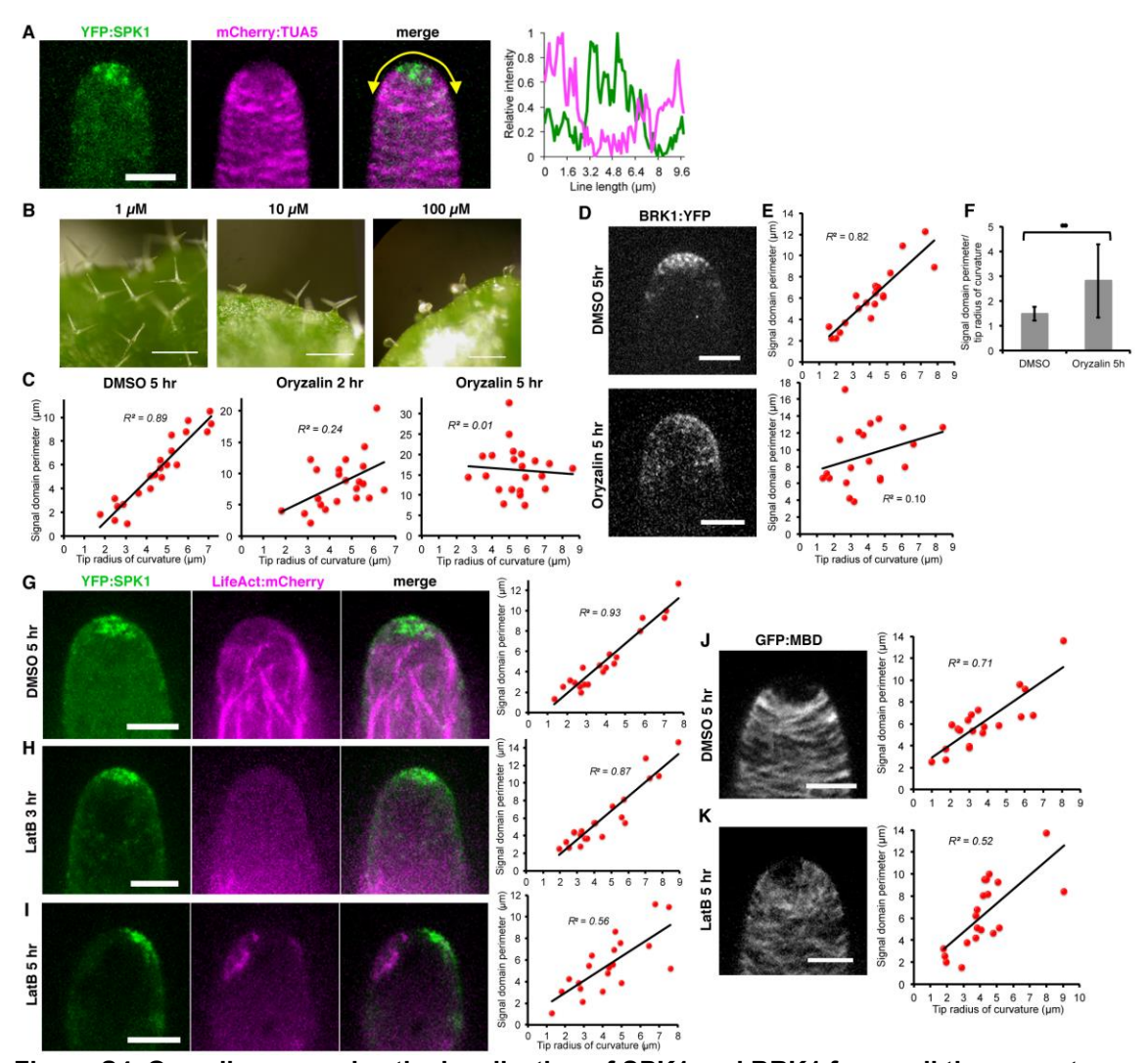


Figure S4. Oryzalin uncouples the localization of SPK1 and BRK1 from cell tip geometry, and actin cytoskeleton appears to have an indirect effect on the SPK1 domain and MDZ, Related to Figure 4.

(A) YFP:SPK1 localizes within an apical microtubule-depletion zone. Right, intensity plot of cortical YFP:SPK1 and mCherry:TUA5 signal along the cell periphery below the yellow line. (B) Trichomes treated with 1 µM oryzalin did not show any obvious phenotype. Some trichomes had a reduced branch number, swollen and short branches after 10 µM oryzalin treatment. Following 100 µM oryzalin treatment most trichomes showed phenotypes such as heavily swollen like a balloon, reduced cell length and branch number. Scale bars represent 200 µm. (C) The correlation between size of the SPK1-positive apical domain and cell geometry was disrupted after 2 hrs of oryzalin treatment. Perimeter length of the SPK1 signal domain was plotted as a function of tip radius of curvature. R2 values were decreased after oryzalin treatment. (D-F) Microtubules restrict BRK1 within the apical-domain. BRK1:YFP localization after 5 hours of DMSO or oryzalin treatment (D). Scale bars represent 5 µm. Scatter plot and correlation coefficient between the BRK1 signal domain perimeter and tip radius of curvature was disrupted after oryzalin treatment (E). Mean size of the BRK1 domain after 5 h of incubation with either mock control buffer or oryzalin (F). Apical-domain perimeter of BRK1:YFP was normalized to tip radius of curvature increased following oryzalin treatment. Mean  $\pm$  SD (n = 20). \*\*P < 0.01 (t test). (G) SPK1 localization and actin organization after 5 hours of DMSO treatment. There was a strong correlation between the size of the SPK1-positive domain and cell geometry, right of image panels. (H) After 3 hours of latrunculin B (LatB) treatment, actin filaments were mostly depolymerized and vacuole invaded the branch apex, which is a characteristic of arp2/3 mutants [S3]. The correlation of the SPK1 domain and cell shape was still strong. (I) After 5 hours of LatB treatment, a concentrated SPK1-positive domain was still present, but was off-center in some cells and the correlation of the SPK1 domain and cell shape was reduced. Some actin bundles always remained in cells throughout the experiments. (J and K) LatB affects geometry of microtubule-depletion zone only after extended time periods. Microtubule localization after 5 hours of DMSO or LatB treatment (J). Correlation between signal domain perimeter and tip radius of curvature was slightly disrupted after extended LatB treatment (K). Scale bars indicate 5 µm.

Marker	Background	Tip signal (%)	n	Ref.		
YFP:SPK1	WT*	96	56			
CRIB:GFP	Col	45	56			
BRK1:YFP	WT*	66	55	[S5]		
ARP2/3:GFP	WT*	28	123	[S5]		
CRIB:GFP	spk1-1	24	34			
YFP:SPK1	sra1	98	47			
YFP:SPK1	arpc2	97	32			
BRK1:YFP	sra1	0	52			
*Rescued line is shown as WT.						

Table S1. Percentage of developing trichome branches showing tip signal, Related to Figures 1 and 2.

Marker	No cortical signal (%)	Apical flank signal (%)	Off axis signal (%)	Normal tip signal (%)	n
BRK1:YFP	54.3	19.6	8.7	17.4	46
ARP2/3:GFP	84.4	11.1	4.4	0.0	43

Table S2. Various patterns of BRK1:YFP and ARP2/3:GFP in young *spk1* trichomes, Related to Figure 2.

### Supplemental References:

- S1. Gutierrez, R., Lindeboom, J.J., Paredez, A.R., Emons, A.M., and Ehrhardt, D.W. (2009). Arabidopsis cortical microtubules position cellulose synthase delivery to the plasma membrane and interact with cellulose synthase trafficking compartments. Nat. Cell Biol. 11, 797-806.
- S2. Vermeer, J.E., van Leeuwen, W., Tobena-Santamaria, R., Laxalt, A.M., Jones, D.R., Divecha, N., Gadella, T.W., Jr., and Munnik, T. (2006). Visualization of PtdIns3P dynamics in living plant cells. Plant J. 47, 687-700.
- S3. Basu, D., Le, J., El-Essal Sel, D., Huang, S., Zhang, C., Mallery, E.L., Koliantz, G., Staiger, C.J., and Szymanski, D.B. (2005). DISTORTED3/SCAR2 is a putative araidopsis WAVE complex subunit that activates the Arp2/3 complex and is required for epidermal morphogenesis. Plant Cell *17*, 502-524.
- S4. Nelson, B.K., Cai, X., and Nebenfuhr, A. (2007). A multicolored set of in vivo organelle markers for co-localization studies in Arabidopsis and other plants. Plant J. *51*, 1126-1136.
- S5. Yanagisawa, M., Desyatova, A.S., Belteton, S., Mallery, E.M., Turner, J.A., and Szymanski, D.B. (2015). Patterning mechanisms of cytoskeletal and cell wall systems during leaf trichome morphogenesis. Nat. Plant *1*, 15014.